

Two-dimensional binary halftoned optical intensity channels

M.D.A. Mohamed and S. Hranilovic

Abstract: The capacity of two-dimensional (2D) optical intensity channels in which transmit images are constrained to be binary-level has been considered. Examples of such links exist in holographic storage, page-oriented memories, optical interconnects, 2D barcodes as well as multiple-input/multiple-output wireless optical links. Data are transmitted by sending a series of time-varying binary-level optical intensity images from transmitter to receiver. Neither strict spatial alignment between transmitter and receiver nor independence among the spatial channels is required. The approach combines spatial discrete multitone modulation developed for spatially frequency selective channels with halftoning to produce a binary-level output image. Data are modulated in spatial frequency domain as dictated by a water pouring spectrum over the optical transfer function as well as channel and quantisation noise. A binary-level output image is produced by exploiting the excess spatial bandwidth available at the transmitter to shape quantisation noise out of band. A general mathematical framework has been presented, in which such systems can be analysed and designed. In a pixelated wireless optical channel application, halftoning achieves 99.8% of the capacity of an equivalent unconstrained continuous amplitude channel using 1megapixel arrays.

1 Introduction

Information is transmitted through optical intensity channels by modulating the instantaneous intensity of an optical source. For two-dimensional (2D) optical channels, the transmitted signal is a 2D intensity image and, as a result, must have non-negative amplitudes. Moreover, the average transmitted power is given by the average image amplitude rather than the average square amplitude as in conventional electrical channels. As a result of these amplitude constraints, the direct application of conventional signalling theory is seldom efficient.

Such 2D optical intensity channels have been used in a variety of applications such as holographic data storage [1–3], page-oriented optical recording [4, 5], 2D barcodes [6, 7] and multiple-input/multiple-output (MIMO) wireless optical communications [8–11]. A major practical problem of many of these applications is the requirement of strict alignment between the transmitter and the receiver in order to avoid the inter-channel interference [1, 2, 12]. Such a system is termed ‘pixel matched’, that is, each receive pixel images a single transmit pixel. Another practical limitation is the constraint on the average and peak optical power transmitted, which is particularly important in applications where the optical signal can interfere with humans, as the case with MIMO wireless optical communications [8].

Recently, a signalling technique, which provides high spectral efficiencies without the need for strict spatial alignment, has been introduced for 2D intensity channels

[13, 14]. The only requirement is that the transmitter array is in the field-of-view of the receiver. Inter-channel interference is in fact modelled and exploited at the transmitter and receiver through the use of spatio-temporal coding. The channel considered in [13, 14] is a class of MIMO wireless optical channels, and is termed pixelated wireless optical channel. In this previous work, the transmitter array is assumed to be able to generate multiple (e.g. 256) intensity levels. Additionally, the non-negativity constraint of the generated image is not considered explicitly, rather, amplitudes are clipped to ensure that the constraints are met.

In this paper, we extend the earlier work on pixelated wireless optical channel to the general case of 2D optical intensity channels by considering transmitter arrays, that is, spatial light modulators (SLMs), in which each pixel is able to output a binary-level intensity, that is on or off. Such transmitters are far simpler than those previously assumed, and can be operated at very high frame rates. The non-negativity constraint is treated explicitly through the design of modified halftoning algorithms. Thus, excess degrees of freedom in spatial frequency domain are exploited to provide binary-level output images, which satisfy all amplitude constraints while maintaining the relaxation on strict spatial alignment.

2 2D optical intensity channels

2.1 Channel model

The transmitter is an SLM consisting of a 2D array of pixels, while the receiver consists of a 2D array of photodiode pixels. The receiver samples the spatial distribution of the optical intensity wavefront incident on its surface. Examples of imaging-type receivers are arrays of photodiodes, charge coupled device cameras and CMOS imagers. Several such arrays have been constructed for free-space and indoor wireless optical communications [15, 16],

as well as for high-speed imaging applications with rates near 10 kframes/s for arrays of over 10^5 pixels [17].

We assume that imaging optics are employed, and that the optical axes of the transmitter and the receiver are aligned such that the receive image $r(u, v)$ is an orthographic projection of the transmit image $x(u, v)$, where (u, v) are continuous spatial coordinates. According to scalar diffraction theory, the impact of the imaging system as well as the shape of transmit and receive pixels can be well modelled as a spatial low-pass filter. This low-pass filter is characterised by its point-spread function (PSF) [18]. That is, the PSF is the optical impulse response of the system, which is modelled as a linear space-invariant system. Therefore the channel model can be written as

$$r(u, v) = x(u, v) \otimes h(u, v) + z(u, v) \quad (1)$$

where $h(u, v)$ is the channel PSF, $z(u, v)$ the channel noise and \otimes 2D linear convolution. The channel model in (1) is a generalisation of a previous model used in holographic data storage [3] and 2D optical recording [4], where the channel was modelled as a finite-extent 2D linear filter that represents the optical blur, or the 2D inter-symbol interference. The same model was used in wireless optical communication applications as well [13, 14].

Two channel amplitude constraints are imposed on $x(u, v)$: (i) a non-negativity constraint, $x(u, v) \geq 0$, that stems from the fact that the transmitted signal is an optical intensity signal, and (ii) $\mathbb{E}\{x(u, v)\} \leq P$, where P is the average optical power and \mathbb{E} is the expectation operator.

2.2 Spatial discrete multitone modulation

Discrete multitone (DMT) is a modulation scheme developed for frequency selective channels. Spatial discrete multitone (SDMT) modulation is the generalisation of DMT to 2D spatial frequency [14]. An appealing advantage is that SDMT is insensitive to the receiver sampling phase, and hence, strict alignment between the transmitter and the receiver is not necessary.

Let the transmit image be $N_1 \times N_2$ pixels and let X be the discrete Fourier transform (DFT) of the transmit image. The complex data to be transmitted are loaded in the complex frequency bins $X(k_1, k_2)$. Hermitian symmetry $X(k_1, k_2) = X^*(N_1 - k_1, N_2 - k_2)$ must be satisfied in order to guarantee real transmit images. According to this model, the transmit images are periodic in space. The receive image is equal to the linear convolution of the transmit image and the channel PSF. By appending a cyclic extension [14, 19] around the image, whose size is at least half the channel memory, the periodicity assumption of the DFT is satisfied, and equalisation is a complex multiplication per spatial frequency bin. In this case, the channel model (1) can be simplified in discrete spatial frequency domain (k_1, k_2) as

$$R(k_1, k_2) = X(k_1, k_2)H(k_1, k_2) + Z(k_1, k_2) \quad (2)$$

where $R(k_1, k_2)$, $X(k_1, k_2)$, $H(k_1, k_2)$ and $Z(k_1, k_2)$ are the DFTs of the receive image, transmit image, PSF and channel additive Gaussian noise, respectively. Thus, the channel can be considered as a number of parallel Gaussian channels in spatial frequency domain, and the aggregate capacity, in the absence of amplitude constraints, is maximised by a water pouring algorithm over the spatial frequency channels [14].

Owing to the non-negativity amplitude constraint of the spatial intensity domain, pouring power to the spatial frequency channels is not straight forward, and does not necessarily maximise the capacity [13, 14]. The complexity of this

technique is increased since it requires an SLM capable of outputting a continuous range of intensities with a high dynamic range, as is noted in electrical DMT systems.

3 Binary-level 2D optical channels

In an effort to reduce the complexity of the transmitter, we confine our consideration to SLMs with binary-level output. Binary-level signalling over the 2D optical wireless channel simplifies not only the SLM design, but also ensures that the channel non-negativity constraint can easily be met since dark/bright pixels are only transmitted over the channel.

Two popular examples of such binary-level SLMs include digital micro-mirror devices (DMD) and arrays of vertical-cavity surface-emitting lasers (VCSELs). Commercial DMD can operate at switching speeds of nearly 10 kHz with array sizes of 2048×1152 mirrors [20]. A 540-element array with 1080 VCSELs has been produced for optical interconnect in which each pixel can be modulated in excess of 200 Mbps [21]. An integrated solid-state array of transceivers has been designed to operate at 155 Mbps/pixel, where arrays of resonant cavity light emitting diodes are bonded to arrays of CMOS driver circuits [22].

The high frame rates permit many channel uses per second, while the large number of pixels gives many spatial degrees of freedom. Since the PSF of the channel is typically spatially low pass, it is not possible to transmit data in high spatial frequency modes as these modes are effectively filtered by the channel. The high-frequency modes are termed the out-of-band region, whereas the low-frequency modes, which carry independent data, are termed the in-band region. In this section, we propose a method that utilises these out-of-band spatial modes to satisfy the channel non-negativity constraint by producing binary-level output images, while achieving high communication rates that approach the rates of unconstrained continuous SLM transmission.

3.1 Digital image halftoning

In image processing, digital image halftoning is defined as the process of converting a continuous-tone image to a binary-level one, which is perceptually close to the original continuous image [23, 24]. The perceptual quality of the image is dominated by the low spatial frequency region since the human visual system is more sensitive to this region of the spectrum. Therefore the power spectral density (PSD) of the quantisation noise is shaped to the high spatial frequency region where the human visual system is not sensitive.

Error diffusion halftoning is the most popular halftoning algorithm first empirically proposed by Floyd and Steinberg [25]. Later, Anastassiou [26] defined a rigorous unifying framework linking $\Delta\Sigma$ modulation and error diffusion halftoning. He showed that the error diffusion algorithm is the extension of $\Delta\Sigma$ modulation to two dimensions, and that both algorithms are oversampled analogue-to-digital converters that rely on the spectral shaping of quantisation noise. The error diffusion system used in this work is surrounded by a dashed box in Fig. 1. The error diffusion feedback filter $j(n_1, n_2)$ was empirically chosen by Floyd, however, others have presented more rigorous designs based on classical filter theory [27]. An all-optical implementation of the error diffusion algorithm has been described in [28], where all pixel quantisation decisions are computed in parallel.

In 2D optical intensity communication channels, the perceptual quality of the transmitted images is not of

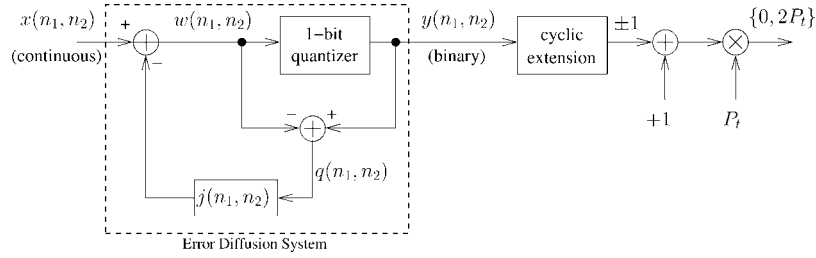


Fig. 1 Half-toned SDMT over 2D optical intensity channels

concern. Instead, the goal is to design a series of images, which maximise the rate at which reliable communication can take place over the channel. Since the channel PSF is analogous to the low-pass human visual system, data are modulated into spatial frequency bins where the channel attenuation is low. Halftoning is then used to produce a binary-level transmit image in which the quantisation noise is shaped to the out-of-band frequency bins that are heavily attenuated by the channel PSF. This high-frequency quantisation noise will be filtered out by the channel and the received image will be a continuous-tone image, which carries the transmitted data along with some residual quantisation noise.

In Fig. 1, let q be the quantiser error, and $\tilde{q} = y - x$ be the closed loop quantisation noise, where x and y are the input continuous-tone image and the output halftoned image, respectively. The analysis of this error diffusion system is not straightforward because the binary-level quantiser is a highly nonlinear element. A conventional assumption is to linearise the quantiser by assuming that the quantiser error q is white with variance σ_q^2 and signal independent [29, 30, Chapter 14]. Once linearised, the following PSD of the quantisation noise \tilde{q} can easily be deduced

$$\begin{aligned}\Phi_{\tilde{q}}(k_1, k_2) &= \Phi_q(k_1, k_2)|1 - J(k_1, k_2)|^2 \\ &= N_1 N_2 \sigma_q^2 |1 - J(k_1, k_2)|^2\end{aligned}\quad (3)$$

where $\Phi_q(k_1, k_2) = N_1 N_2 \sigma_q^2$ is the PSD of the quantiser error, and $J(k_1, k_2)$ is the DFT of the feedback filter. That is, the power of the quantiser error is shaped by the noise power shaping function $|1 - J(k_1, k_2)|^2$.

In order to shape the quantiser error power to the out-of-band region, the error diffusion feedback filter $J(k_1, k_2)$ is chosen to be a unity DC-gain filter such that the noise power shaping function $|1 - J(k_1, k_2)|^2$ will have a null at DC. The total quantisation noise power, in all complex frequency bins, after noise shaping is given by

$$\begin{aligned}\sum_{k_1, k_2} \Phi_{\tilde{q}} &= N_1 N_2 \sigma_q^2 \sum_{k_1, k_2} [1 - J(k_1, k_2)]^* [1 - J(k_1, k_2)] \\ &= (N_1 N_2)^2 \sigma_q^2 (1 + \varepsilon_j - 2j(0, 0))\end{aligned}\quad (4)$$

where

$$\varepsilon_j = \sum_{n_1, n_2} |j(n_1, n_2)|^2$$

is the feedback filter energy, and the fact that $\sum J(k_1, k_2) = N_1 N_2 j(0, 0)$ is used.

Therefore the total quantisation noise power increases with the filter energy ε_j . However, high values of ε_j are not problematic as long as the noise is well shaped to the out-of-band region that is attenuated by the channel PSF. The key point is to maximise the channel capacity,

defined in Section 3.2, and not to minimise the total quantisation noise power.

3.2 Half-toned SDMT modulation

The binary-level SDMT communication system based on halftoning is shown in Fig. 1. The SDMT transmit image is formed as described in Section 2.2, and is the input of the error diffusion system. A cyclic extension is added to the halftoned image and the frame is biased by a constant bias of +1 to satisfy the non-negativity constraint. Finally, the entire frame is multiplied by P_t to scale the output levels to $\{0, 2P_t\}$. Since the input continuous SDMT image $x(n_1, n_2)$ is assumed to be zero mean, the output halftoned binary image $y(n_1, n_2)$ is also zero mean, and hence the average transmit optical power is equal to P_t .

The received image, as given by (2), can be rewritten as

$$\begin{aligned}R(k_1, k_2) &= P_t [X(k_1, k_2) + \tilde{Q}(k_1, k_2) + N_1 N_2 \delta(k_1, k_2)] \\ &\quad \times H(k_1, k_2) + Z(k_1, k_2)\end{aligned}\quad (5)$$

Dividing (5) by $P_t H(k_1, k_2)$ yields

$$\begin{aligned}\frac{R(k_1, k_2)}{P_t H(k_1, k_2)} &= [X(k_1, k_2) + N_1 N_2 \delta(k_1, k_2)] \\ &\quad + \tilde{Q}(k_1, k_2) + \tilde{Z}(k_1, k_2)\end{aligned}$$

where

$$\tilde{Z}(k_1, k_2) = \frac{Z(k_1, k_2)}{P_t H(k_1, k_2)}$$

is the effective channel Gaussian noise.

That is, the effective received image is equal to a DC-biased version of the transmit image contaminated by two noise components: $\tilde{Q}(k_1, k_2)$ and $\tilde{Z}(k_1, k_2)$ whose PSDs are $\Phi_{\tilde{q}}(k_1, k_2)$ and $\Phi_z(k_1, k_2)$, respectively. By further assuming that the quantiser error is Gaussian, then $\Phi_{\tilde{q}}(k_1, k_2) + \Phi_z(k_1, k_2)$ defines the Gaussian noise ‘bowl’ over which the total available electrical power is poured in order to maximise the aggregate channel capacity. If $\Phi_{\tilde{q}}(k_1, k_2) \gg \Phi_z(k_1, k_2)$ in the in-band region, the quantisation noise dominates and the system is termed quantisation noise-limited. On the other hand, if $\Phi_{\tilde{q}}(k_1, k_2) \ll \Phi_z(k_1, k_2)$ in the in-band region, the channel noise dominates and the system is then termed optical power-limited.

Notice that the non-negativity constraint is no longer an issue while pouring power to the bowl $\Phi_{\tilde{q}}(k_1, k_2) + \Phi_z(k_1, k_2)$, as was the case in [13, 14], because the output image is a binary one. Let $\Phi_x(k_1, k_2)$ be the electrical power allocated to the complex frequency bin (k_1, k_2) such that the total frame electrical power is equal to $(1/N_1 N_2) \sum \Phi_x(k_1, k_2) = \sigma_x^2 N_1 N_2$ for some fixed input electrical power σ_x^2 . Then, the aggregate system capacity

C is given by

$$C = \frac{1}{2} \sum_{k_1=0}^{N_1-1} \sum_{k_2=0}^{N_2-1} \log \left(1 + \frac{\Phi_x(k_1, k_2)}{\Phi_q(k_1, k_2) + \Phi_z(k_1, k_2)} \right) \quad (6)$$

where $\Phi_x(k_1, k_2)$ is calculated by the water pouring algorithm to maximise the capacity C [31], and no power is poured to the DC-bin, that is $\Phi_x(0, 0) = 0$, because a constant DC-level of P_t is added to each frame.

Notice that the expression in (6) for the capacity is only valid under the aforementioned assumptions of signal-independent, white, Gaussian quantiser error. The larger the total input signal electrical power, the more likely this assumption is to fail. In Section 3.3, we deduce an upper bound on the total input electrical power and feedback filter energy that are necessary to ensure the consistency of the system model.

3.3 Linearised analytical model

Using the signal-independence and whiteness assumptions of the quantiser error, the variance σ_w^2 of the input to the quantiser can be written as

$$\sigma_w^2 = \sigma_x^2 + \sigma_q^2 \varepsilon_j \quad (7)$$

where σ_x^2 is the average electrical power of the input SDMT signal as shown in Fig. 1.

The availability of some information about the statistical properties of the input SDMT signal can further aid the estimation of the quantiser error power σ_q^2 . The amplitude of DMT signals is known to closely approximate Gaussian distributed noise [32, Section 3.3]. Therefore from the Gaussianity assumption of the quantiser error, the input w to the quantiser is Gaussian distributed as well, and the quantiser error power is given by

$$\begin{aligned} \sigma_q^2 &= \int_{-\infty}^0 f_w(w) (-1-w)^2 dw + \int_0^{\infty} f_w(w) (1-w)^2 dw \\ &= 1 + \sigma_w^2 - \frac{4\sigma_w}{\sqrt{2\pi}} \end{aligned} \quad (8)$$

where $f_w(w)$ is a zero-mean Gaussian probability density function with variance σ_w^2 . Solving (7) and (8) for σ_w

$$\sigma_w = \frac{-\sqrt{2/\pi} + \sqrt{2/\pi + (1/\varepsilon_j - 1)(1 + \sigma_x^2/\varepsilon_j)}}{1/\varepsilon_j - 1} \quad (9)$$

Therefore σ_q^2 can be estimated from knowledge of σ_x^2 using (8) and (9). For σ_w to be real, the discriminant under the square root in (9) must be positive, and hence, the following upper bound on σ_x^2 exists when $\varepsilon_j > 1$

$$\sigma_x^2 \leq \varepsilon_j \left[\frac{2}{\pi(1 - 1/\varepsilon_j)} - 1 \right] \quad (10)$$

Since $\sigma_x^2 \geq 0$, then so too is the right-hand side of (10). Hence, we have the following upper bound on the feedback filter energy ε_j

$$\varepsilon_j \leq \frac{\pi}{\pi - 2} \simeq 2.75 \quad (11)$$

That is, for our model to be consistent with the assumptions made, the feedback filter energy cannot exceed 2.75, and the input electrical power cannot exceed the bound in (10) when $\varepsilon_j > 1$.

4 Example: pixelated wireless optical channel

In this section, a specific example of a 2D optical communication channel, namely, the pixelated wireless optical channel, is studied. The pixelated wireless optical channel is introduced in [13, 14], where each transmitter element is assumed to be able to generate 256 intensity levels. Additionally, the non-negativity constraint of the generated image was not considered explicitly, rather, amplitudes are clipped to ensure non-negativity. In this section, half-toned SDMT is applied to the channel measured in [13, 14], and the obtained channel capacity is compared to the results of [13, 14]. In Section 4.1, the channel parameters are defined. The error diffusion feedback filter is designed in Section 4.2, and numerical results and discussion are presented in Section 4.3.

4.1 Simulation setup

In Section 3.1, it was assumed that the quantiser error is white and signal independent with variance σ_q^2 . Similarly, it is assumed in our simulations that the channel noise is white, Gaussian, and signal independent with variance σ_z^2 . Therefore the PSD of the effective noise \tilde{Z} is equal to

$$\Phi_z(k_1, k_2) = \frac{\sigma_z^2 N_1 N_2}{|P_t H_0 H(k_1, k_2)|^2} = \frac{N_1 N_2}{|\rho H(k_1, k_2)|^2} \quad (12)$$

where H_0 is the DC-gain of the unity DC-gain PSF, $H(k_1, k_2)$, and

$$\rho = \frac{P_t H_0}{\sigma_z} \quad (13)$$

Substituting from (3) and (12) in (6), the capacity is equal to

$$\begin{aligned} C &= \frac{1}{2} \sum_{k_1=0}^{N_1-1} \sum_{k_2=0}^{N_2-1} \log \left(1 + \frac{\Phi_x(k_1, k_2)}{N_1 N_2} \left/ \left[\sigma_q^2 |1 - J(k_1, k_2)|^2 \right. \right. \right. \\ &\quad \left. \left. \left. + |\rho H(k_1, k_2)|^{-2} \right] \right) \end{aligned} \quad (14)$$

Notice that the system is quantisation noise-limited if $\rho \gg 1/\sigma_q$ and is optical power-limited if $\rho \ll 1/\sigma_q$.

In our simulations, we have assumed that both the transmitter and receiver have the same number of pixels and that spatial synchronisation is achieved through appropriate scaling of the imaging optics [14]. Therefore the transmitter and receiver have the same spatial Nyquist region. The transmitted image is required to be in the field-of-view of the receiver, while strict alignment between the transmitter and the receiver is not necessary. The simulations are done for a square frame $N_1 = N_2 = N$, and a unity DC-gain Gaussian PSF

$$H(k_1, k_2) = \exp \left(-\frac{k_1^2}{2w_{h_1}^2} - \frac{k_2^2}{2w_{h_2}^2} \right) \quad (15)$$

where w_{h_1} and w_{h_2} are measures of the PSF widths. In all simulations, the channel parameters are taken from a measured pixelated wireless optical channel [14], and the parameters are presented in Table 1.

All the measurements presented in Table 1 were done for a single receiver array with $N = 154$ pixels. For a given imager size, increasing the value of N by a factor α

Table 1: Measured parameters of a pixelated wireless optical channel in [13, 14]

N	w_{h_1}	w_{h_2}	ρ
154	41.01	41.85	56.05

Measured ρ is a worst case, calculated at the highest noise variance measured in [13, 14]

implies a corresponding decrease in the pixel area by a factor α^2 . This in turn results in (i) decreasing the DC-gain of the PSF, that is H_0 , by α^2 , and (ii) decreasing the channel noise power, that is σ_z^2 , by α^2 . This can be attributed to the fact that both the average optical power collected by the pixel and the pixel noise variance are proportional to the pixel area [33, 34]. Notice that the PSF in (15) is the product of the transmitter pixel shape, the imaging optics transfer function, and the receiver pixel shape [14]. In light of (13), ρ decreases by a factor of α , and the following appropriate scaling of ρ is used during simulations

$$\rho_N = \frac{\rho_{154}}{\alpha} = \rho_{154} \times \frac{154}{N} \quad (16)$$

where ρ_N is the value of ρ when the imager is $N \times N$ pixels, and ρ_{154} is the value of ρ when the imager is 154×154 pixels, given in Table 1. Notice that the effect of changing the pixel area on the bandwidth of the PSF is negligible due to the very small pixel size.

4.2 Halftoning design

In this example, the following form for the error diffusion feedback filter is proposed

$$j(n_1, n_2) = \begin{bmatrix} 0 & a \\ a & 1 - 2a \end{bmatrix} \longleftrightarrow J(k_1, k_2) \quad (17)$$

This filter is symmetric, causal, has unity DC-gain, and is among the simplest feedback filters that can be used for digital halftoning. The short length of the filter makes it faster and less complex to implement in real time. Another attractive feature is that a single parameter, a , indexes the entire family of filters. In this case

$$\varepsilon_j = \sum |j(n_1, n_2)|^2 = 6a^2 - 4a + 1 \quad (18)$$

Substituting from (18) in the bound (11), a is restricted to the interval

$$-0.3 < a < 0.968 \quad (19)$$

in order for our model to be consistent. Higher values of $|a|$ can saturate the binary-level quantiser and hence affects the stability of the error diffusion system in Fig. 1.

A cross-section for $k_1 = k_2$ through the noise power shaping function $|1 - J(k_1, k_2)|^2$ is plotted for different values of a in Fig. 2. It is straight forward to show that for $a = 1/3$, ε_j is minimised. Consequently, $a = 1/3$ minimises the total quantisation noise power, in (4). From the figure, it is also clear that maximising a is desirable, within (19), in order to widen the low quantisation noise region around DC. Recall that the goal is to minimise the residual quantisation noise in the spatial frequency bins which carry data, rather than minimising the total quantisation noise power. Thus, $a = 1/3$ is not necessarily the best choice for J .

As the electrical power σ_x^2 increases, so too does the dynamic range of the input and the likelihood of quantiser

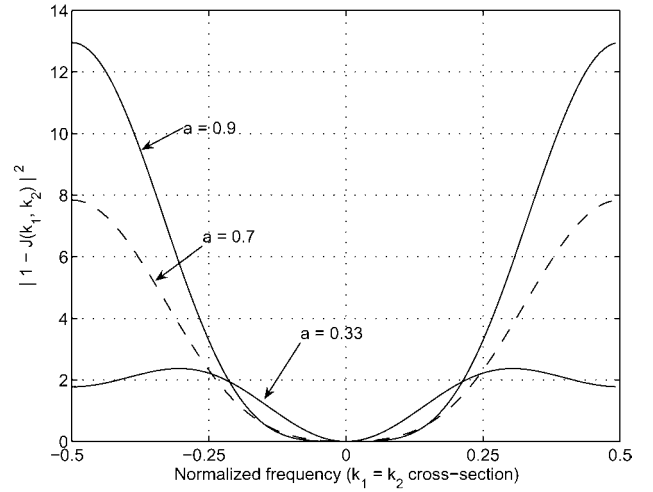


Fig. 2 Cross-sections of the noise power shaping function, $|1 - J(k_1, k_2)|^2$, for $k_1 = k_2$ and a variety of feedback filter parameters a

saturation and system instability. When $a > 2/3$, $\varepsilon_j > 1$ and the bound in (10) is necessary. In the simulation results that follow, $\sigma_x^2 = 0.1$ is used, which satisfies the upper bound (10) for all values of a considered.

An example of a continuous-tone image is shown in Fig. 3 for $N = 512$, along with the corresponding halftoned image and their spectra. The complex data to be transmitted are loaded to the low-frequency bins of the continuous-tone image as implied by the water pouring allocation. By comparing the spectra in Figs. 3c and d, it is evident that the data can be recovered from the low-frequency region of the halftoned binary-level image. A great majority of the quantisation noise power is shaped to the out-of-band region, which is indicated by the four high-power corners of the halftoned image spectrum. In this case, the system is optical power-limited as the

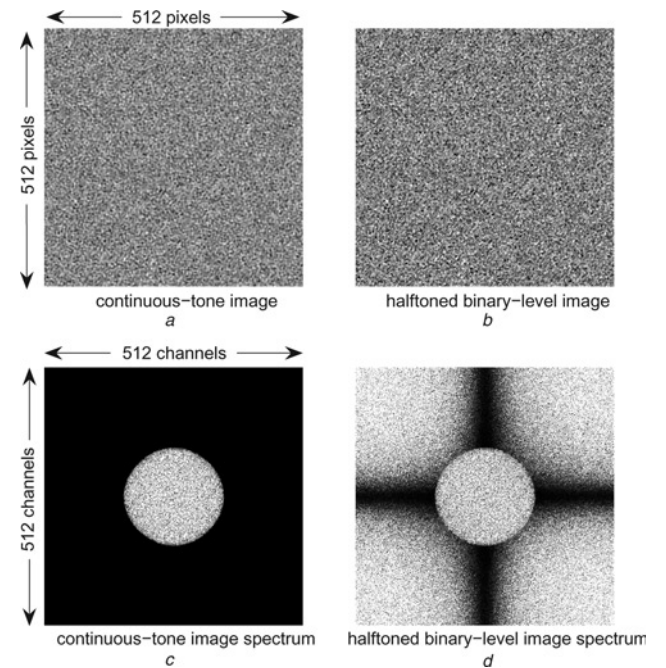


Fig. 3 Optical power-limited system

a Continuous-tone image
 b Corresponding halftoned image
 c Spectrum of continuous-tone image
 d Spectrum of halftoned image
 $N = 512$, $a = 0.9$, $\sigma_x^2 = 0.1$, w_{h_1} and w_{h_2} as given in Table 1, and ρ as given by (16)

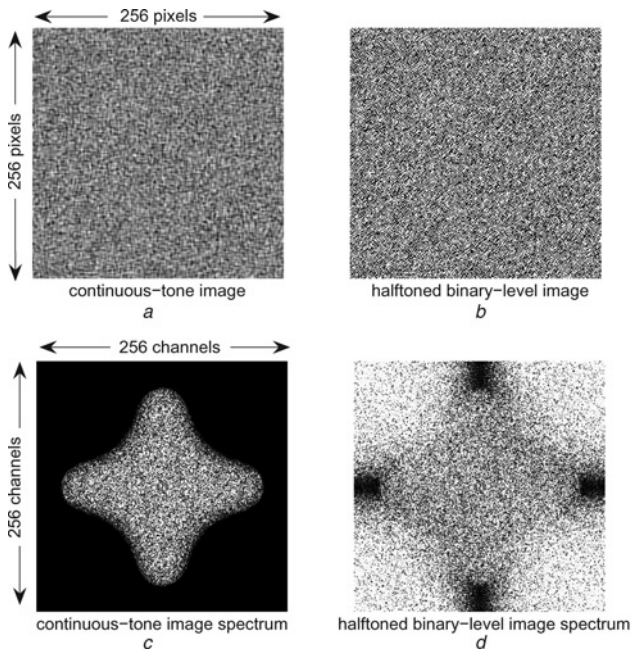


Fig. 4 Quantization noise-limited system

- a Continuous-tone image
- b Corresponding halftoned image
- c Spectrum of continuous-tone image
- d Spectrum of halftoned image

$N = 256$, $a = 0.9$, $\sigma_x^2 = 0.1$, w_{h_1} and w_{h_2} as given in Table 1, and ρ as given by (16)

effect of quantisation noise is mild, and the shape of the in-band power allocation is dominated by the PSF.

A similar example is shown in Fig. 4 for $N = 256$. In this case, the system is quantisation noise-limited due to the reduced number of out-of-band spatial modes to which quantisation noise can be shaped. As a result, the shape of the in-band power allocation is dominated by the quantisation noise shaping function $|1 - J(k_1, k_2)|^2$. Qualitatively, data cannot fully be recovered from the low-frequency region of the spectrum of the halftoned image because of the in-band quantisation noise. As will be shown in Section 4.3, the reduction in capacity resulting from reducing N from 512 to 256 is nearly 51.7%.

Notice that the capacity of the halftoned SDMT system, or any finite-level SDMT system, is upper bounded by that of a continuous SDMT transmitter with the same σ_x^2 neglecting the non-negativity amplitude constraints. This upper bound is given by (14) with $\sigma_q^2 = 0$.

4.3 Discussion

In this section, the capacity of the halftoned SDMT system is calculated for $\sigma_x^2 = 0.1$ and the system parameters given in Table 1 by two different procedures: (i) by using our linearised model to estimate σ_q^2 , as in (8), and (ii) by simulations, where $\Phi_{\hat{q}}(k_1, k_2)$ is estimated by averaging over 1000 randomly generated frames. Notice that the measured quantisation noise PSD, $\Phi_{\hat{q}}(k_1, k_2)$, affects the water pouring bowl which in turn affects the power allocation over the complex frequency bins which again impacts the quantisation noise. As a result, the iterative scenario shown in Fig. 5 is used during simulations to allow $\Phi_{\hat{q}}(k_1, k_2)$ to converge to the correct value for power allocation.

The results obtained from our linearised analytical model are compared to simulations in Fig. 6. It is evident that both model and simulations are in close agreement. Notice the capacity increases with the number of pixels N^2 . This is

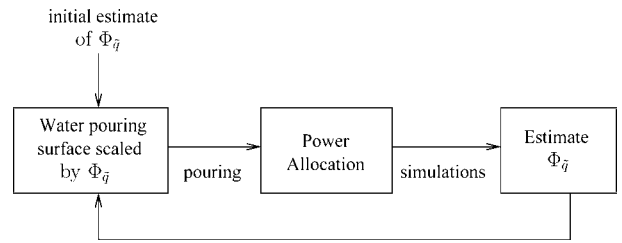


Fig. 5 Iterations used in simulations to evaluate $\Phi_{\hat{q}}(k_1, k_2)$ and the power allocation

due to the fact that the size of the out-of-band region increases with N , and hence the quantisation noise can be shaped further from the data bearing region as in Figs. 3 and 4. However, the capacity saturates to a limiting value as N increases. This is due to the fact that, although the number of channels increases as N^2 , the signal-to-noise ratio (proportional to ρ^2) decreases at the same rate as in (16). Additionally, larger values of a lead to high channel capacities. This is due to the fact seen in Fig. 2, that larger a allows for lower residual quantisation noise in the band of interest. Notice however, as implied by (10), as a increases, σ_x^2 must decrease to ensure stability of the halftoning modulator.

Fig. 6 compares the capacity of the halftoned SDMT system to an upper bound obtained by employing a continuous unconstrained SDMT transmitter with the same σ_x^2 . The gap between the capacities of the binary-level transmission and the continuous-amplitude transmission diminishes as N increases. This gap approaches zero in the limit $N \rightarrow \infty$ as the in-band quantisation noise also approaches zero on this limit. Thus, for a given PSF, increasing the number of excess spatial degrees of freedom allows a binary-level SDMT transmitter to approach the same capacity as the optical power-limited regime.

Fig. 6 also compares the capacity of the halftoned SDMT system to that of the experimental 256-level SDMT system measured in [14] at $N = 154$. The coded rate achieved in [14] is also indicated at the same value of N . The binary-level system with $a = 0.9$ achieves 57.37% of the capacity of the 256-level system for $N = 154$. Thus, for small N , quantisation noise-limited channels benefit greatly from

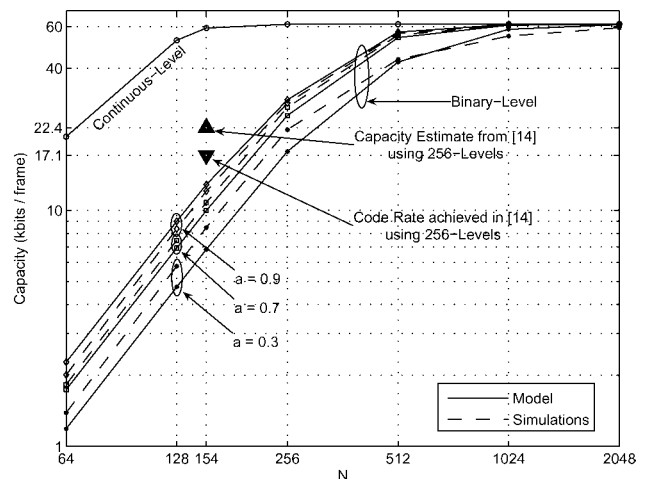


Fig. 6 Capacity of the pixelated channel against $N = N_1 = N_2$ with $\sigma_x^2 = 0.1$

Results of the linearised analytical model in Section 3.3 are compared to those from simulations, and to those of a continuous SDMT transmitter without non-negativity constraint. The capacity estimate (Δ) and code rate (∇) achieved in [14] using 256-level transmitter are also shown at $N = 154$

multi-level output. The capacity of the continuous system is an upper bound for both the 256-level and the binary systems. At higher values of N , the capacity of the binary system approaches the continuous-amplitude upper bound. For instance, the binary system ($a = 0.9$) achieves $\sim 92.6\%$ of the upper bound at $N = 512$, and nearly 99.8% at $N = 1024$. This suggests that employing more than two quantisation levels is not necessary as N gets large, because the system is optical power-limited in this case, and quantisation noise is effectively shaped out-of-band.

5 Conclusions

The capacity and data rates of point-to-point 2D optical intensity channels can be significantly improved by using spatial degrees of freedom. In this work, we have considered the design of these channels in which only binary-level optical intensity transmitters are used. The approach proposed combines SDMT modulation with halftoning ideas from image processing. Using a simple error diffusion filter, we demonstrate that the capacity of the channel using a binary-level transmitter approaches that when using an idealised continuous transmitter that is capable of transmitting positive and negative amplitudes. In practice, the capacities reported here could be approached using spatio-temporal coding of the data bins, as was done in [14] for a pixelated wireless optical channel. However, our goal in this work was to demonstrate that the fundamental limits of pixelated channels with binary-level transmission are significant and merit continued study.

Currently, a prototype binary-level pixelated channel is being constructed by the authors using a DMD SLM with 1024×768 elements [20] and a mega-pixel CMOS imager. Additionally, reduced complexity coding and decoding techniques for these channels are also being explored to permit real-time operation. Potential applications of such intensity channels include holographic storage, page-oriented memories, optical interconnects, 2D barcodes and MIMO wireless optical links.

6 References

- Shelby, R.M., Hoffnagle, J.A., Burr, G.W., Jefferson, C.M., Bernal, M.-P., Coufal, H., Grygier, R.K., Gunther, H., Macfarlane, R.M., and Sincerbox, G.T.: 'Pixel-matched holographic data storage with megabit pages', *Optics Lett.*, 1997, **22**, (19), pp. 1509–1511
- Burr, G.W., Ashley, J., Coufal, H., Grygier, R.K., Hoffnagle, J.A., Jefferson, C.M., and Marcus, B.: 'Modulation coding for pixel-matched holographic data storage', *Optics Lett.*, 1997, **22**, (9), pp. 639–641
- Nabavi, S., and Kumar, B.V.K.V.: 'Detection methods for holographic data storage'. Proc. IEEE Optical Data Storage Topical Meeting, 23–26 April 2006, Montreal, QC, Canada, pp. 156–158
- Siegel, P.H.: 'Information-theoretic limits of two-dimensional optical recording channels'. Proc. IEEE Optical Data Storage Topical Meeting, 23–26 April 2006, Montreal, QC, Canada, pp. 165–167
- Huang, L., Mathew, G., and Chong, T.C.: 'Channel modeling and target design for two-dimensional optical storage systems', *IEEE Trans. Magn.*, 2005, **41**, (8), pp. 2414–2424
- Villán, R., Voloshynovskiy, S., Koval, O., and Pun, T.: 'Multilevel 2-D bar codes: toward high-capacity storage modules for multimedia security and management', *IEEE Trans. Inf. Forensics Secur.*, 2006, **1**, (4), pp. 405–420
- Claycomb, W., and Shin, D.: 'Using a two dimensional colorized barcode solution for authentication in pervasive computing'. Proc. ACS/IEEE Int. Conf. on Pervasive Services, Lyon, France, 26–29 June 2006, pp. 173–180
- Kahn, J.M., and Barry, J.R.: 'Wireless infrared communications', *Proc. IEEE*, 1997, **85**, (2), pp. 263–298
- O'Brien, D.C., Quasem, S., Zikic, S., and Faulkner, G.E.: 'Multiple input multiple output systems for optical wireless: Challenges and possibilities', *Proc. SPIE*, 2006, **6304**, pp. 630 416-1–630 416-7
- Faucher, J., Venditti, M.B., and Plant, D.V.: 'Application of parallel forward-error correction in two-dimensional optical-data links', *IEEE/OSA J. Lightwave Technol.*, 2003, **21**, (2), pp. 466–475
- Plant, D.V., and Kirk, A.G.: 'Optical interconnects at the chip and board level: challenges and solutions', *Proc. IEEE*, 2000, **88**, (6), pp. 806–818
- Bisaillon, E., Brosseau, D.F., Yamamoto, T., Mony, M., Bernier, E., Goodwill, D., Plant, D.V., and Kirk, A.G.: 'Free-space optical link with spatial redundancy for misalignment tolerance', *IEEE Photon. Technol. Lett.*, 2002, **14**, (2), pp. 242–244
- Hranilovic, S., and Kschischang, F.R.: 'Short-range wireless optical communication using pixelated transmitters and imaging receivers'. Proc. IEEE Int. Conf. on Communications, 20–24 June 2004, Paris, France, vol. 2, pp. 891–895
- Hranilovic, S., and Kschischang, F.R.: 'A pixelated MIMO wireless optical communication system', *IEEE J. Sel. Topics Quantum Electron.*, 2006, **12**, (4), pp. 859–874
- Leibowitz, B.S., Boser, B.E., and Pister, K.S.J.: 'CMOS smart pixel for free-space optical communication', *Proc. SPIE*, 2001, **4306A**, pp. 21–26
- O'Brien, D.C., Gaulkner, G.E., Jim, K., Zyamba, E.B., Edwards, D.J., Whitehead, M., Stavrinou, P., Parry, G., Bellon, J., Sibley, M.J., Lalithambika, V.A., Joyner, V.M., Samsudin, R.J., Holburn, D.M., and Mears, R.J.: 'High-speed integrated transceivers for optical wireless', *IEEE Commun. Mag.*, 2003, **41**, (3), pp. 58–62
- Kleinfelder, S., Lim, S., Liu, X., and Gamal, A.E.: 'A 10kframe/s 0.18 μm CMOS digital pixel sensor with pixel-level memory'. Proc. IEEE Int. Solid-State Circuits Conf., 4–8 February 2001, San Francisco, CA, USA, pp. 88–89
- Goodman, J.: 'Introduction to Fourier optics' (McGraw-Hill, 1968, 1st edn.)
- Peled, A., and Ruiz, A.: 'Frequency domain data transmission using reduced computational complexity algorithms'. Proc. IEEE Int. Conf. Acoustics, Speech, and Signal Processing, 9–11 April 1980, Denver, CO, USA, vol. 5, pp. 964–967
- Texas Instruments Digital Light Processing. <http://www.dlp.com>
- Venditti, M.B., Laprise, E., Faucher, J., Laprise, P.-O., Lugo, J.E.A., and Plant, D.V.: 'Design and test of an optoelectronic-VLSI chip with 540-element receiver-transmitter arrays using differential optical signaling', *IEEE J. Sel. Topics Quantum Electron.*, 2003, **9**, (2), pp. 361–379
- O'Brien, D.C., Faulkner, G.E., Zyambo, E.B., Jim, K., Edwards, D.J., Stavrinou, P., Parry, G., Bellon, J., Sibley, M.J., Lalithambika, V.A., Joyner, V.M., Samsudin, R.J., Holburn, D.M., and Mears, R.J.: 'Integrated transceivers for optical wireless communications', *IEEE J. Sel. Topics Quantum Electron.*, 2005, **11**, (1), pp. 173–183
- Ulichney, R.: 'Digital halftoning' (MIT Press, Cambridge, MA, USA, 1987)
- Shoop, B.L.: 'Photonic analog-to-digital conversion' (Springer-Verlag, Berlin, Germany, 2001)
- Floyd, R.W., and Steinberg, L.: 'An adaptive algorithm for spatial gray scale'. SID Symp. Digest, Society for Information Display, 1975, pp. 36–37
- Anastassiou, D.: 'Error diffusion coding for A/D conversion', *IEEE Trans. Circuits Syst.*, 1989, **36**, (9), pp. 1175–1186
- Shoop, B.L., and Ressler, E.K.: 'An error diffusion neural network for digital image halftoning'. Proc. IEEE Workshop on Neural Networks for Signal Processing, 31 August–2 September 1995, pp. 427–436
- Shoop, B.L., and Ressler, E.K.: 'Optimal error diffusion for digital halftoning using an optical neural network'. Proc. IEEE Int. Conf. on Image Processing, 13–16 November 1994, Austin, TX, USA, vol. 2, pp. 1036–1040
- Norsworthy, S.R., Schreier, R., and Temes, G.C. (Eds.): 'Delta-sigma data converters: theory, design, and simulation' (Wiley-IEEE Press, NY, USA, 1996)
- Johns, D.A., and Martin, K.W.: 'Analog integrated circuit design' (John Wiley & Sons, 1996, 1st edn.)
- Cover, T.M., and Thomas, J.A.: 'Elements of information theory' (John Wiley & Sons, NY, USA, 1991, 1st edn.)
- Tellado, J.: 'Multicarrier modulation with low PAR: applications to DSL and wireless' (Kluwer Academic Publishers, Norwell, MA, USA, 2000)
- Chen, T., Catrysse, P., Gamal, A.E., and Wandell, B.: 'How small should pixel size be?'. Proc. SPIE Electronic Imaging Conf., San Jose, CA, USA, January 2000, vol. 3965
- Holst, G.C.: 'CCD arrays, cameras, and displays' (SPIE Optical Engineering Press, Bellingham, WA, USA, 1998, 2nd edn.)